Multiaxial fatigue damage modelling at Macro scale of Ti6AL4V alloy

A.K. Marmi[a]*, L. Duchne[a]†, A.M. Habraken[a]‡

[a]University of Liege, Chemin des Chevreuils 1, 4000 Liege, Belgium.

Abstract

Lemaitre and Chaboche fatigue model is investigated in order to predict the fatigue life of tensile samples with and without notch defining different stress concentration fields. Elastoplastic FE simulations based on anisotropic yield locus description were carried out in order to obtain the stress and strain distributions near the notch root. The Lemaitre and Chaboche fatigue model was applied with the point method and the gradient method.

Keys Words : fatigue damage, notch, stress gradient, fatigue life

1. Introduction

Mainly two different ways are possible to predict the safety of aeronautical pieces. Either a direct use of SN curves information and stress fields knowledge in the pieces allow verifying the soundness of the piece design (old classical simplified way) or the SN curves allow the identification and the validation of a damage fatigue model that is applied to the actual piece stress state (alternative approach). Of course, if the fatigue model used in this alternative approach is validated, it can also generate new SN curves used in the classical way. In this paper, the finite element (FE) simulations of SN curves for Ti-6Al-4V notched and unnotched specimens are based on the fatigue model of continuum damage mechanics developed by Lemaitre and Chaboche. A first application of this model on the notched or unnotched specimens in tensile state (see section 8.2) demonstrates that if the data set is identified with the unnotched specimen, the model predictions for the notched case are very far from the experiments, too short life times are computed. The model provides too conservative results. An easy solution is to modify the material data and in this case the notched case experimental results can also be simulated with accuracy. However the interest of a model is poor if you must modify its material data for each geometry. Physical sound models assume a unique set of parameters for one material.

The current research introduces the stress gradient effect in the formulation of the Lemaitre and Chaboche damage model.

Once the elastoplastic constitutive law was identified for the studied material (section 3), the next step was the identification of the damage model of Lemaitre and Chaboche from some SN curves of the unnotched specimen (section 5). Other SN curves were computed to validate the predictive capacity of the model. Then using the same material data set, the Lemaitre and Chaboche model was improved by a gradient method used to predict the fatigue life of notched specimens in tensile fatigue tests (section 8).

2. Material

The Ti-6Al-4V alloy produced by Timet company was used in the present fatigue experiments, and in the fatigue tests of the Handbook [1] for V-notch and unnotched samples. The chemical composition and the mechanical properties are pre-

*amarmi@ulg.ac.be
†L.Duchene@ulg.ac.be
‡Anne.Habraken@ulg.ac.be

sented in Tables 1 and 2. The heat treatment for the used Ti-6Al-4V plate consisted of an annealing process at 760^o for 1 hour. Its microstructure contains both an alpha phase, and a lamellar beta phase (Figure 1). The lattice of the apha phase is an hexagonal closed packed one and the beta phase is body centered cubic. The apha content is approximately 85 %.

Fe	V	Al	C	O	N	Y	H	O+2N
0.14	4.0	6.26	0.008	0.18	0.004	< 0.0004	58	0.19

TAB. 1
Chemical composition of Ti-6Al-4V alloy (in weight percent)

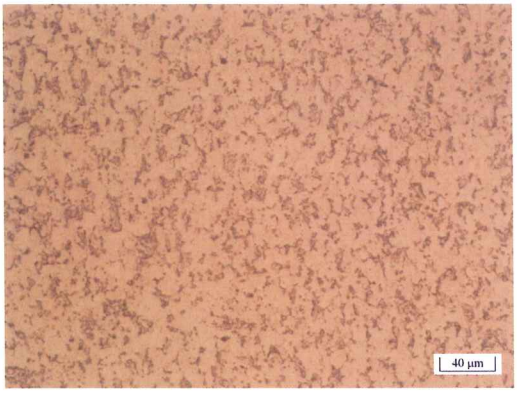

Figure 1. Optical micrograph of two phase microstructure of the Ti-6Al-4V annealed plate

Ti-6Al-4V property	annealed	aged
Yield Stress (MPa)	940	1080
Ultimate Stress (MPa)	1040	1180
Elastic modulus (GPa)	109.4	109.4

TAB. 2
Mechanical properties of annealed Ti-6Al-4V plate : for the samples of the present work, unnotched Handbook samples, V-notched Handbook samples and for solution-treated and aged Ti-6Al-4V for the holed plate

3. Constitutive law

3.1. Elastic behavior and Hill anisotropic yield locus

The elastic behavior is defined by the well known Hooke's law (Young's modulus is 109.4 MPa and Poisson's ratio is 0.37). The yield function is described by the anisotropic Hill yield locus. The Hill anisotropic equivalent stress is computed as a function of the Cauchy stress tensor $\boldsymbol{\sigma}$ and the fourth order material tensor $\mathbf{H}$:

$$\sigma_{eq,Hill} = \sqrt{\boldsymbol{\sigma} : \mathbf{H} : \boldsymbol{\sigma}} \tag{1}$$

Or using a Voigt notation :

$$\sigma_{eq,Hill} = \sqrt{\sigma_i H_{ij} \sigma_j} \text{ i,j=1,..,6}$$

where σ_j are the components of the stress state expressed as a six-component vector $[\sigma_{11}, \sigma_{22}, \sigma_{33}, \sigma_{12}, \sigma_{13}, \sigma_{23}]$. H_{ij} is the 6x6 anisotropic material matrix obtained from $\mathbf{H}$. It is assumed constant during the loading. The material constants (see Table 3) are determinated from uniaxial tensile tests along different directions (RD, TD and 45^O direction), and simple shear tests along RD. H_{ij} is written in the form :

$$H_{ij} = \begin{pmatrix} G+H & -H & -G & 0 & 0 & 0 \\ -H & H+F & -F & 0 & 0 & 0 \\ -G & -F & F+G & 0 & 0 & 0 \\ 0 & 0 & 0 & 2N & 0 & 0 \\ 0 & 0 & 0 & 0 & 2L & 0 \\ 0 & 0 & 0 & 0 & 0 & 2M \end{pmatrix} \tag{2}$$

3.2. Teodosiu-Hu hardening law

In order to predict the fatigue life of the specimens subjected to constant cyclic loading, a representative behavior law of Ti-6Al-4V is required to compute the stress field which is an input of the fatigue model. The Teodosiu and Hu hardening model is an advanced model able to predict the Bauschinger effect and other transient hardening phenomena observed during two-stage

	Value	Unit
F	0.54	—
G	0.34	—
H	0.65	—
N	2.34	—
M	2.34	—
L	2.34	—

TAB. 3
Material parameters of Hill yield locus

sequential rheological tests. It is based on physical considerations, mainly the description of the evolution of the so-called planar persistent dislocation structures (PPDS) and their contribution to the hardening of the material. The yield surface is described by the following equation :

$$F(\boldsymbol{\sigma}, \mathbf{X}, \mathbf{P}, \mathbf{S}, R) = \sigma_{eq,Hill}(\boldsymbol{\sigma} - \mathbf{X}) - R_0 - Y - m|\mathbf{S}| \quad (3)$$

Here, the equivalent Hill stress is function of $\boldsymbol{\sigma}$ and the back stress tensor $\mathbf{X}$; R_0 and Y are the initial yield stress and the isotropic hardening stress. $\mathbf{S}$ is a fourth order tensor describing the directional strength of planar dislocations structures. $m|\mathbf{S}|$ represents the contribution of the PPDS to the isotropic hardening. $\mathbf{P}$ is a second-order tensor that depicts the polarity of the persistent dislocation structures. The consideration of a non-linear kinematic hardening is of primordial importance in order to have a good description of the cyclic plastic behaviour of the Ti-6Al-4V alloy. The evolution of the kinematic hardening, is characterized by the evolution rule for the back stress $\mathbf{X}$ (similar to Armstrong-Frederick back stress evolution [2]) :

$$\dot{\mathbf{X}} = C_X(X_{SAT}\mathbf{n} - \mathbf{X})\dot{\bar{\varepsilon}}^{pl} \quad (4)$$

where $\dot{\bar{\varepsilon}}^{pl}$ is the equivalent plastic strain rate. C_X is a material parameter described in Table 4. $\mathbf{n}$ is the saturation direction, it is equal to $(\frac{\boldsymbol{\sigma}-\mathbf{X}}{\sigma_{eq,Hill}})$. The variable X_{SAT} depends on the internal state variable $\mathbf{S}$ through the following equation :

$$X_{SAT} = X_{SAT0} + (1-m)|\mathbf{S}|\sqrt{q + (1-q)\beta_S^2} \quad (5)$$

where X_{SAT0}, m, q are material parameters (see Table 4). β_S $(= \frac{S_D}{|\mathbf{S}|})$ measures the change in orientation of the current strain rate tensor with respect to the PPDS. The internal state variable $\mathbf{S}$ is decomposed into two parts : a scalar part S_D (the dislocation structure associated to the currenly active slip systems), and a fourth order tensor part $\mathbf{S}_L$ related to the latent part of the persistent dislocation structures. The decomposition equation of $\mathbf{S}$ is :

$$\mathbf{S} = S_D\mathbf{N} \otimes \mathbf{N} + \mathbf{S}_L \quad (6)$$

where $\mathbf{N} = \mathbf{d}^p/|\mathbf{d}^p|$ represents the plastic strain rate direction, $\mathbf{d}^p$ is the plastic strain rate tensor. The evolution equations of S_D and $\mathbf{S}_L$ are given respectively by :

$$\dot{S}_D = C_{SD}[g(S_{SAT} - S_D) - h(\mathbf{X}, \mathbf{N}, \mathbf{n})S_D]\dot{\bar{\varepsilon}}^{pl} \quad (7)$$

$$\dot{\mathbf{S}_L} = -C_{SL}\left(\frac{Z}{S_{SAT}}\right)^{n_L}\mathbf{S}_L\dot{\bar{\varepsilon}}^{pl} \quad (8)$$

with

$$Z = |\mathbf{S}_L| = \sqrt{|\mathbf{S}| - S_D^2} \quad (9)$$

where S_{SAT}, C_{SD}, C_{SL} and n_L are material parameters (see Table 4). The functions g and h help to capture transient hardening after a strain path change. Their expressions are :

$$g = \begin{cases} \{1 - \frac{C_p}{C_{SD}+C_p}|\frac{S_D}{S_{SAT}} - \mathbf{P}:\mathbf{N}| & \text{if } P_D \geq 0 \\ (1+P_D)^{n_p}(1 - \frac{C_p}{C_{SD}+C_p})\frac{S_D}{S_{SAT}} & \text{otherwise} \end{cases} \quad (10)$$

where, $P_D = \mathbf{P}:\mathbf{N}$

$$h = \frac{1}{2}(1 - \frac{\mathbf{X}:\mathbf{N}}{X_{SAT}\mathbf{n}:\mathbf{N}}) \quad (11)$$

with C_p and n_p material constants.

The evolution law for the polarity tensor is :

$$\dot{\mathbf{P}} = C_p(\mathbf{N} - \mathbf{P})\dot{\bar{\varepsilon}}^{pl} \tag{12}$$

The size of the yield surface is defined by the isotropic hardening variable Y. It is a function of the accumulated plastic deformation $\bar{\varepsilon}^{pl}$ using a simple exponential law :

$$R = R_{SAT}(1 - exp(-C_R\bar{\varepsilon}^{pl})) \tag{13}$$

where R_{SAT} and C_R are material constants (see Table 4). The value of R_{SAT} takes a positive value for a cyclic hardening material, and a negative value for a cyclic softening material (Ti-6Al-4V is a softening material under cyclic loading).

The set of 13 material parameters of the Teodosiu and Hu model are obtained by calibration on the Ti-6Al-4V plate. They are presented in Table 4. The number of material parameters for this hardening model is large and some parameters are clearly dedicated only to some events (stagnation of hardening in reverse test, in orthogonal tests...). Details of the identification procedure can be found in [3].

4. Experiments

The High Cycle Fatigue data (HCF) used in this study come either from our tests (Ulg tests), or from the Handbook [1]. The geometry of the unnotched fatigue tests of the present work is represented in Figure 2. Two types of plate notched specimens were tested : the first one is a V-notch (Figure 3a), and the second one is a plate with a central hole (Figure 3b).

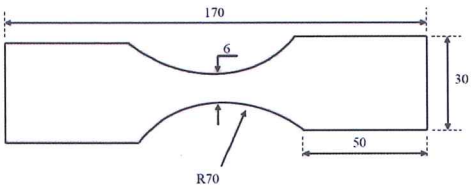

Figure 2. Unnotched Ti-6Al-4V specimen geometry (present study, dimensions in mm)

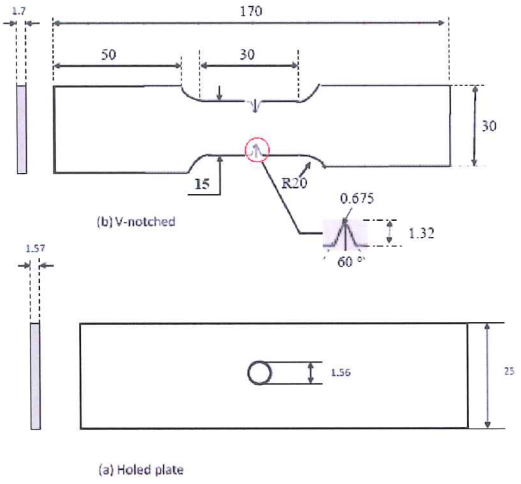

Figure 3. Notched Ti-6Al-4V specimen, (a) V-notch, (b) Holed plate (from [1]), all dimensions in mm

The V-notched specimen has a notch depth h of 1.32 mm, the V-notch angle β is equal to 60^o, the notch radius ρ is 0.675 mm. The plate thickness t is 1.7 mm for the V-notched specimen of the Handbook [1] and 2.5 mm for the present study. The sample reduced width is equal to 15 mm. This shape of V-notched specimens corresponds to an elastic stress concentration factor K_t of 3.3 according to the graphs of Noda [4]. The holed plate is 1.57 mm in thickness with a 1.56 mm hole diameter. Its K_t value is 2.8.

The HCF tests were conducted at stress ratios R $(= \frac{\sigma_{min}}{\sigma_{max}})$ of 0.1, 0.5, -0.5 and -1, where σ_{min} and σ_{max} are respectively the minimum and maximum stress during the load cycle. A sinusoidal loading at the cyclic frequencies of 60-100 Hz was applied. The fatigue tests were conducted to obtain the SN curves. The mainly analyzed domain is ranging from 10^4 to 10^7 cycles.

The SN experimental results for unnotched and notched specimens are presented in section 8, together with the simulation results predicted by the fatigue model.

Parameter	Value	Unit	Description
C_p	0.34	—	characterizes the polarization rate of the PPDS
n_p	10.23	—	
C_{SD}	10	—	characterizes the saturation rate of **S**
C_X	26.41	—	characterizes the saturation rate of the back stress **X**
X_{SAT0}	235.00	MPa	represents the saturation value of the back stress **X**
m	0.3	—	defines the contribution of the PPDS to the isotropic hardening
S_{SAT0}	190.00	MPa	represents the saturation value of **S**
n_L	0.00	—	characterizes the saturation rate of $\mathbf{S}_L$
q	0	—	
R_0	945	MPa	initial yield stress
C_R	15	—	characterizes the saturation rate of the isotropic hardening stress Y
R_{SAT}	-175	MPa	represents the saturation value of the isotropic hardening stress Y
C_{SL}	0.00	—	

TAB. 4
Material parameters of Teodosiu-Hu hardening law

5. Continuum fatigue damage model

5.1. Uniaxial non-linear cumulative fatigue damage model

It is possible to predict the fatigue life of the specimen or mechanical component by using a fatigue damage approach. A useful fatigue damage model is the one proposed by Lemaitre and Chaboche [5], where the evolution of the damage is nonlinear versus time (which is confirmed by experimental observations), and the increment of damage depends on loading parameters (mean stress, stress amplitude...). Assuming an istropic damage evolution for the material, the damage tensor **D** is reduced to a scalar variable : $\mathbf{D} = D \cdot \mathbf{I}$, where **I** is the second order identity tensor. In 1D cyclic loading, the fatigue cumulative damage model describing the deterioration of the material microstructure under cyclic plasticity is formulated by :

$$\frac{dD}{dN} = [1-(1-D)^{\beta+1}]^{\alpha(\sigma_{max},\bar{\sigma})} \cdot [\frac{\sigma_{max}-\bar{\sigma}}{M(\bar{\sigma})(1-D)}]^{\beta} \quad (14)$$

D is the damage scalar variable and N the number of cycles. σ_{max}, $\bar{\sigma}$ are respectively the maximum and mean stress. The function $\alpha(\sigma_{max},\bar{\sigma})$ links the damage to the cyclic loading :

$$\alpha(\sigma_{max},\bar{\sigma}) = 1 - a\langle\frac{\sigma_{max}-\sigma_l(\bar{\sigma})}{\sigma_u-\sigma_{max}}\rangle \quad (15)$$

The fatigue limit $\sigma_l(\bar{\sigma})$ depends on the mean stress by the following relation :

$$\sigma_l(\bar{\sigma}) = \sigma_{l0} + \bar{\sigma}(1-b_1\sigma_{l0}) \quad (16)$$

σ_{l0} and σ_u are respectively the fatigue limit at zero mean stress and the ultimate tensile stress. The brackets $\langle u\rangle$ are defined as $\langle u\rangle = 0$ if $u \leq 0$ and $\langle u\rangle = u$ if $u > 0$.

The function $M(\bar{\sigma})$ quantifies the mean stress effect through Low Cycle Fatigue (LCF) loading range :

$$M(\bar{\sigma}) = M_0(1-b_2\bar{\sigma}) \quad (17)$$

In Equations (14) to (18), β, M_0, b_1, b_2 and a are material parameters determined from fatigue tests. The number of cycles to failure N_R under a constant loading amplitude is obtained by integrating Equation (14) from D=0 (initial undamaged state) to D=1(macrocrack initiation) :

$$N_R = \frac{1}{1+\beta}\frac{1}{aM_0^{-\beta}}\frac{\langle\sigma_u-\sigma_{max}\rangle}{\langle\sigma_a-\sigma_l(\bar{\sigma})\rangle} \cdot (\frac{\sigma_a}{1-b_2\bar{\sigma}})^{-\beta} \quad (18)$$

where σ_a is the stress amplitude during the cycle loading.

For this study, the influence of the damage on the deformation is assumed to be weak. Therefore, the mechanical behavior law and the damage accumulation analysis are decoupled. This assumption allows considerable computation simplifications because, in fatigue life prediction, the amplitude of the stresses is used to determine the loading cycle.

5.2. Multiaxial cumulative fatigue damage model

The applied stress and strain tensors are often multiaxial and present a complex path during a loading cycle. In the case of multiaxial loading fatigue, cumulative damage models are very few in the literature and lack of experimental verification. The Lemaitre and Chaboche model has been extended to 3D loading by Chaudonneret [6]. The evolution of damage in the case of multiaxial applied stress is represented by the following equation :

$$\frac{dD}{dN} = [1-(1-D)^{\beta+1}]^{\alpha(..)} \cdot \left[\frac{A_{II}}{M_0(1-3b_2\sigma_{H,mean})(1-D)}\right]^{\beta} \quad (19)$$

where A_{II} is the amplitude of octahedral shear stress and $\sigma_{H,mean}$ is the mean hydrostatic stress defined by $\sigma_{H,mean} = \frac{1}{6}[max(tr(\boldsymbol{\sigma})) + min(tr(\boldsymbol{\sigma}))]$ with $tr(\boldsymbol{\sigma}) = \sigma_{11} + \sigma_{22} + \sigma_{33}$. The exponent $\alpha(..)$ is now defined by Equation (20), where $\sigma_{eq,Hill,max}$ is the maximum Hill equivalent stress during the loading cycle.

$$\alpha(A_{II}, \sigma_{H,mean}, \sigma_{eq,Hill,max}) = 1 - a\langle\frac{A_{II} - A^*_{II}}{\sigma_u - \sigma_{eq,Hill,max}}\rangle \quad (20)$$

The Sines [6] fatigue limit criterion is formulated by the following equation :

$$A_{II} = \sigma_{l0}(1 - b_1\sigma_{H,mean}) \quad (21)$$

In the case of multiaxial fatigue loading, an infinite fatigue life is obtained if the stress amplitude A_{II} respects :

$$A_{II} \leq A^*_{II} = \sigma_{l0}(1 - b_1\bar{\sigma}_{H,mean}) \quad (22)$$

The term describing the stactic facture in 1D loading $(\sigma_u - \sigma_{max})$ in Equation (15) is replaced by $(\sigma_u - \sigma_{eq,Hill,max})$ in 3D loading case (Equation (20)).

For the proportional loading, the stress amplitude A_{II} is defined by :

$$A_{II} = \frac{1}{2}\sqrt{\frac{2}{3}(S_{ijmax} - S_{ijmin})(S_{ijmax} - S_{ijmin})} \quad (23)$$

where S_{ijmax} and S_{ijmin} are the maximum and the minimum values of the deviatoric stress tensor during the loading cycle.

$\sigma_{eq,Hill,max}$ has the following expression (maximum value for one cycle) :

$$\sigma_{eq,Hill,max} = max[H(\sigma_{11} - \sigma_{22})^2 + G(\sigma_{11} - \sigma_{33})^2 + F(\sigma_{22} - \sigma_{33})^2 + 2N\sigma_{12}^2 + 2L\sigma_{13}^2 + 2M\sigma_{23}^2] \quad (24)$$

By integration of Equation (19), the number of cycles to failure N_R for multiaxial loading is :

$$N_R = \frac{1}{1+\beta} \cdot \frac{1}{aM_0^{-\beta}} \frac{\langle\sigma_u - \sigma_{eq,Hill,max}\rangle}{\langle A_{II} - A^*_{II}\rangle} \cdot \left[\frac{A_{II}}{1 - b_2\sigma_{H,mean}}\right]^{-\beta} \quad (25)$$

The material parameters : β, $aM_0^{-\beta}$ of the Lemaitre and Chaboche model are determined by using fatigue tests of smooth specimens ($K_t = 1$), and SN curve with zero mean stress. The other coeffients b_1 and b_2 are determined from other SN curves with non zero mean stresses (see Table 5).

σ_{l0} and σ_u are respectively equal to 358 MPa, and 1040 MPa for the annealed Ti-6Al-4V, while σ_u is 1180 MPa for the Ti-6Al-4V aged plate.

β	$aM_0^{-\beta}$	b_1	b_2
1.79	1.79×10^{-11}	0.0013	0.00055

TAB. 5
Material parameters of Lemaitre and Chaboche fatigue damage model

6. Simulations

6.1. Mesh and plate thickness effect on K_t

The home-made finite element code Lagamine [8] was used. The first step in the numerical computations was the determination of the mesh density required at the notch root to get a converged solution independent of the mesh size. This analysis was performed in elasticity with two element layers through the thickness. The final mesh consisted of 2200 BWD3D [9] finite elements for the V-notched specimen (Figure 5) and 2240 elements for the holed plate specimen (Figure 6). BWD3D is a mixed type hexahedral brick finite element, with one integration point. The FE simulations were used to calculate the stress distribution near the notch root.
The stress concentration factor is defined by : $\sigma_{xx,max}/\sigma_{net}$, where $\sigma_{xx,max}$ is the opening stress at the notch tip (at the present analysis, K_t takes at the first Gauss point ahead of the notch root), σ_{net} is the mean stress of the net section on the ligament $(W - 2 \cdot h)$.

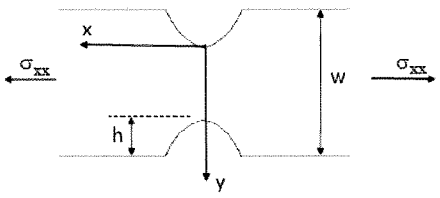

Figure 4. Illustration of the problem in the x-y plane for V-notch

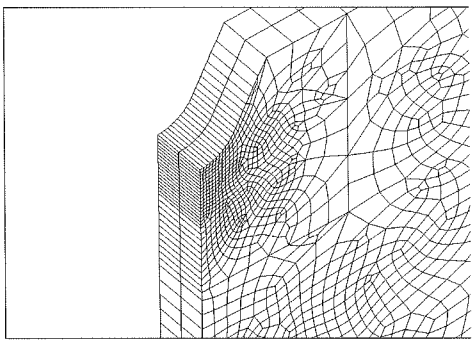

Figure 5. Finite element mesh for the V-notched specimen (only one eight is modelled due to symmetry)

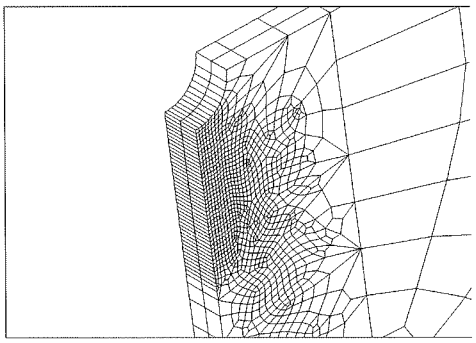

Figure 6. Finite element mesh for the holed specimen (only one eight is modelled)

Figure 7 shows the stress concentration factor K_t variation versus the distance from the mid-thickness plane. K_t values were obtained from linear elastic FE analysis with four element layers (the plate thickness is 1.7mm). K_t value decreases from the mid-thickness to the surface of the specimen, the minimum K_t value is located at the specimen surface.

The elastic stress distribution at notch roots was noticeably studied using FE analysis and analytical formula like Chen formula (Equation 26) and USAMI formula (Equation 27). The results

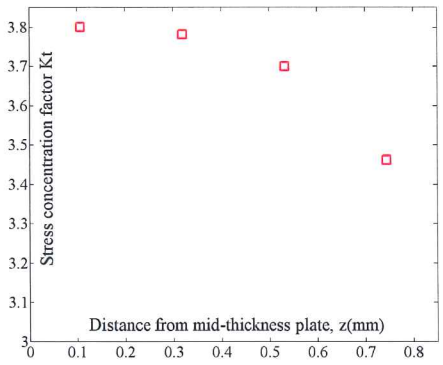

Figure 7. K_t values variation along plate thickness

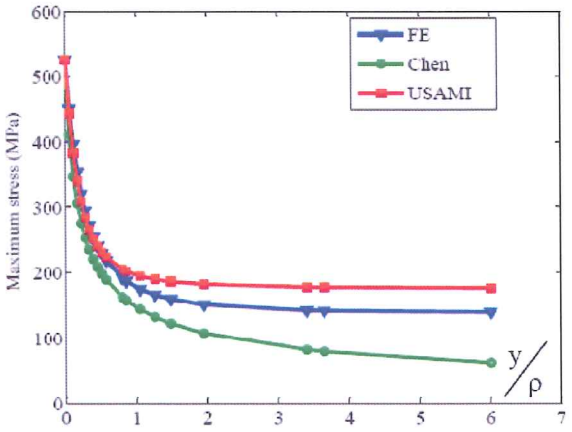

Figure 8. Elastic axial stress distribution (the abscissa is the ratio of the distance from the notch tip to notch radius)

are plotted in Figure 8. The USAMI formula is very close to the FE stress distribution for a small distance from the notch tip and they diverge near the specimen center. Chen formula gives a bad stress distribution.

$$\sigma_{xx}(y) = \sigma_{xx,max}\sqrt{\frac{\rho}{\rho + 8y}} \tag{26}$$

$$\sigma_{xx}(y) = \frac{\sigma_{xx,max}}{3}[1 + \frac{1}{2}(1 + \frac{y}{\rho})^{-2} + \frac{3}{2}(1 + \frac{y}{\rho})^{-4}] \tag{27}$$

In Equations (26) and (27), $\sigma_{xx,max}$ is the maximum stress value at the notch tip, y is the distance from the notch tip and ρ is the notch radius.

Finite element simulations of the behaviour at notch root using the Teodosiu hardening+Hill yield locus were used to model cyclic plasticity. Figure 9 shows the four stress-strain cycles at notch root for a nominal stress ratio of 0.1. It can be noted that there is an elastic stabilization (elastic shakedown) witch takes place after the first yielding (the first cycle). The first load cycle gives rise to compressive residual stresses at and near the notch tip. The elastic shakedown occurs quickly and the majority of the fatigue life will be

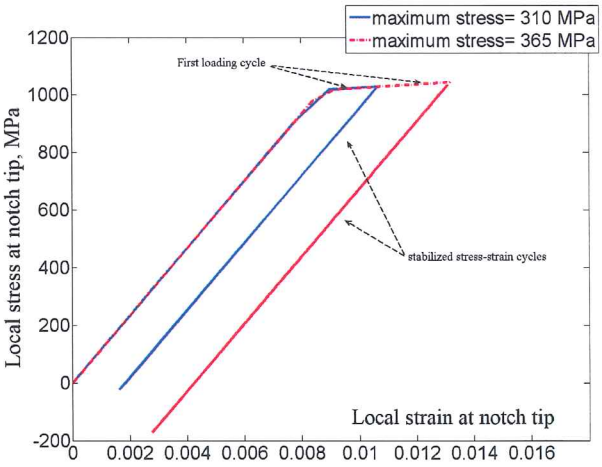

Figure 9. Stress-stain curves at notch tip along the tensile direction for two maximum stresses (stress ratio R=0.1)

generated in the elastic range. In fact, the local plasticity at notch root causes a fatigue damage zone near the notch root (failure zone).

Figure 10 defines the evolution of the load

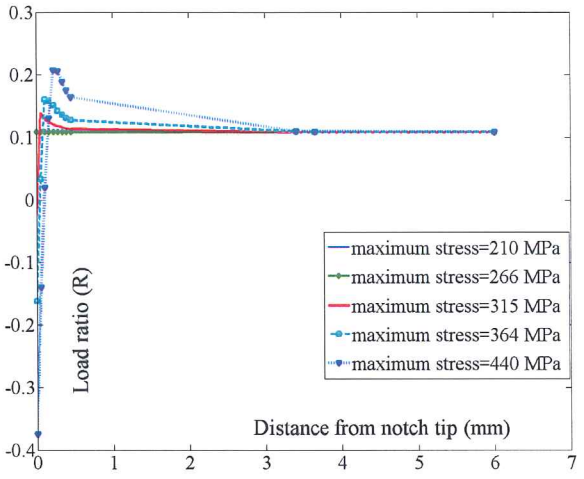

Figure 10. Evolution of the stress ratio versus distance from notch tip, for nominal stress ratio R=0.1, and in the axial direction

stress ratio versus the distance from the notch tip for five applied stresses, for a nominally applied stress ratio of 0.1. We note that near the notch root the load cycle was partly compressive (local stress ratio is negative) and the higher stress level gives rise to a higher compressive part (higher plastic zone). As the distance from notch root increases the local stress ratio reaches a value above the nominal load ration (peak value). Beyond this, the local stress ratio decays towards the nominal stress ratio. For the nominal stress ratio 0.5 there is no compressive part at notch tip, all material point are under tensile loading.

7. Fatigue life prediction for notched samples

This section describes the fatigue life prediction of notched specimens using the fatigue damage model and stress gradient effect. In this study the estimation of fatigue life is based on crack initiation.

7.1. Local method

The local method takes in account only the time history of the stress tensor computed at a point (at the notch tip). The application of the damage model is local. The mentioned method gives a conservative results in the case of non homogeneous stress distribution (stress gradient). It doesn't take the coupled effect of sound and damaged zone influence near the notch root.

7.2. Gradient methods (non local method)

The sustainable maximum local stress in the specimen is not the same in a uniformly stressed specimen as in a notched one. The specimen with a stress concentration will tolerate a higher maximum stress.

Using the maximum equivalent stresses at the notch root gives conservative results. In order to solve this problem, the equivalent stresses can be averaged over a line, over an area (in 2D case) or over a volume (3D).

Papadopoulos [10] used the relative gradient of the maximum hydrostatic tension during a load cycle to modify the Crossland criterion. Nadot and Billaudeau [11] proposed a multiaxial fatigue criterion for surface defective materials. This criterion is based on Crossland formulation and also uses the stress gradient around defect to describe the influence of the stress gradient on fatigue limit.

Yao Weixing [12] introduced the stress intensity to quantify the damaged zone by the following equation :

$$\sigma_{FI} = \frac{1}{V}\int_{\Omega} f(\sigma_{ij})\varphi(r)dv \tag{28}$$

where Ω is the fatigue failure region, V is the volume of Ω, $\varphi(r)$ is the weigh function. $f(\sigma_{ij})$ is the equivalent stress function.

Qylafku et al [13] proposed another approach to compute the damage damage zone using the effective stress σ_{eff} :

$$\sigma_{eff} = \frac{1}{X_{eff}} \int_0^{X_{eff}} \sigma(y) \cdot \phi(y, \chi) dy \quad (29)$$

where X_{eff} is an effective distance (limit of the damage zone), $\phi(y, \chi)$ is the weight function. Qylafku proposed to introduce the fatigue damage zone (used for the evaluation of the effective distance), via the computation of the relative stress gradient $\chi(y)$ (x and y coordinates are defined in Figure 11) :

$$\chi(y) = \frac{1}{\sigma_{xx}(y)} \frac{\partial \sigma_{xx}(y)}{\partial y} \quad (30)$$

For the current study, the generalized Papadopoulos formula (relative stress gradient) is applied to the equivalent stresses used in Lemaitre and Chaboche fatigue model. The amplitude of stress A_{II} and the Hill equivalent stress $\sigma_{eq,Hill,max}$ adjusted by the gradient value are :

$$A_{II}^{G} = A_{II}^{loc} \cdot [1 - a^* \langle \frac{\mathbf{G}_a}{A_{II}^{loc}} \rangle] \quad (31)$$

$$\sigma_{eq,Hill,max}^{G} = \sigma_{eq,Hill,max}^{loc} \cdot [1 - a^* \langle \frac{\mathbf{G}_{Hill}}{\sigma_{eq,Hill,max}^{loc}} \rangle] \quad (32)$$

where A_{II}^{loc} is the value of A_{II} at notch tip, $\sigma_{eq,Hill,max}^{loc}$ is the value of $\sigma_{eq,Hill,max}$ at notch tip. a^* is a parameter used to control how strong the effect of the gradient adjustment is. It has a direct length scale interpretation. It is equal to 0.28 mm for all FE simulations with stress gradient (for V-notch and holed plate).

The purpose is here to calculate the gradient of the A_{II} (G_a)and $\sigma_{eq,Hill,max}(G_{Hill})$ by a definition similar to gradient formula given by Papadopoulos :

$$G_a = [(\frac{\partial A_{II}}{\partial x})^2 + (\frac{\partial A_{II}}{\partial y})^2 + (\frac{\partial A_{II}}{\partial z})^2]^{1/2} \quad (33)$$

$$G_{Hill} = [(\frac{\partial \sigma_{eq,hill,max}}{\partial x})^2 + (\frac{\partial \sigma_{eq,hill,max}}{\partial y})^2 + (\frac{\partial \sigma_{eq,hill,max}}{\partial z})^2]^{1/2} \quad (34)$$

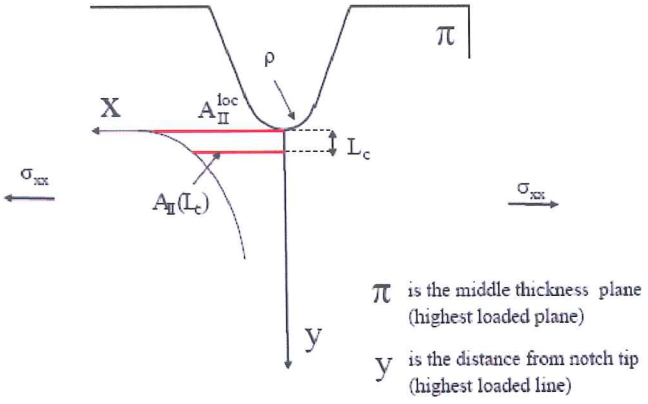

Figure 11. Details of the stress gradient plotted line

We propose to reduce the study of the stress distribution around notch tip to the plotted line 'y' from notch tip (Figure 11). The stress gradient is negligible in x and z directions.
The calculation of the stress gradient of A_{II} and $\sigma_{eq,Hill,max}$ is between notch tip, A_{II}^{loc} and the critical distance L_c, by the following equations :

$$\mathbf{G}_a = \frac{\Delta A_{II}}{\Delta y} = \frac{A_{II}^{loc} - A_{II}(L_c)}{L_c} \quad (35)$$

$$\mathbf{G}_{Hill} = \frac{\Delta \sigma_{eq,Hill,max}}{\Delta y} = \frac{\sigma_{eq,Hill,max}^{loc} - \sigma_{eq,Hill,max}(L_c)}{L_c} \quad (36)$$

where L_c is the critical distance related to the distribution of the triaxiality factor. Its value is introduced in the next section. By increasing the applied load, the A_{II} gradient increases (see Figure 12) and the fatigue life decreases.
The usual triaxiality factor is adapted to the used anisotropic yield locus :

$$TR = \frac{\sigma_{mean}}{\sigma_{eqHill}} \quad (37)$$

where, σ_{mean} is the hydrostatic stress defined by :

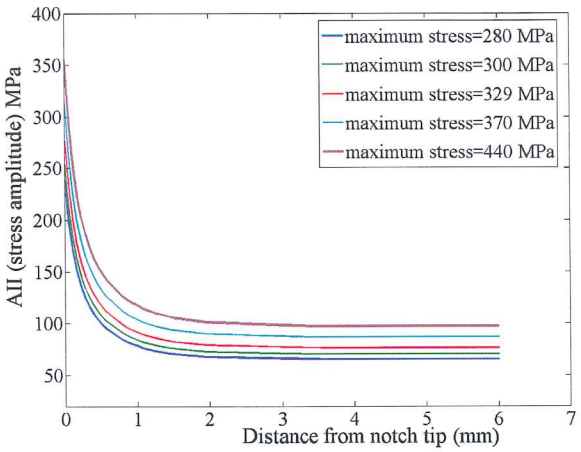

Figure 12. Evolution of A_{II} versus distance from the notch tip, for R=0.5

$$\sigma_{mean} = \frac{1}{3} tr(\boldsymbol{\sigma}) \tag{38}$$

In many models of continuum damage mechanics, the term of triaxiality factor is present, like Lemaitre model [14], Bonora model [15]. As the fatigue life, the damage value is sensitive to its value. This gives an argument to show that the stress triaxiality around the notch tip is an important parameter.

The triaxiality changes with time for cyclic loading. A mean triaxialty factor (TR_{mean}) is defined for loading cycle by :

$$TR_{mean} = \frac{TR_{max} + TR_{min}}{2} \tag{39}$$

where TR_{max} and TR_{min} are the maximum and minimum values of the triaxialty factor during the loading cycle respectively.

The mean triaxiality factor is established to distinguish between fatigue life under multiaxial tension and compression.

Figure 13 shows the distribution of the mean stress triaxiality from the notched tip, its peak value is located at the critical distance (L_c) from the notch tip. The peak value is influenced by the applied load and the stress ratio.

The definition of the critical distance (L_c) for the stress gradient computation is given at the distance located at the maximum value of the mean triaxiaty fator (TR_{mean})(the peak value, see Figure 13) :

$$L_c = L(\frac{dTR(y)}{dy} = 0)$$

The mean hydrostatic stress is averaged over the load plotted line y with the following equation :

$$\sigma^*_{H,mean} = \frac{1}{L_c} \int_0^{L_c} \sigma_{H,mean}(y) dy \tag{40}$$

Note that using the generalized Papadopoulos gradient formula for the mean hydrostatic stress did not give better results. The results given by Equation 40 are better. For a good prediction of fatigue life, its value is averaged over a line. For integration of equation (40), a polynomial stress distribution of $\sigma_{H,mean}(y)$ is adopted for a good fit of the stress value at integrations points :

$$\sigma_{H,mean}(y) = \sum_{i=0}^{n} a_i y^i \tag{41}$$

where, a_i are polynomial coefficients.

The figure 14 shows the distribution of maximum triaxiality factor, its maximum value is at specific distance from notch tip. Figure 15 shows the distribution of Hill equivalent stress around the notch tip.

8. Results and discussion

8.1. Results of the uniaxial case

The curves of Figures 16, 17 and 18 compare the experimental data for unnotched plate specimens ($K_t = 1$) with R=-0.5, R=0.1 and R=0.5, under constant-amplitude loading. The fatigue damage model gives a correct prediction of fatigue

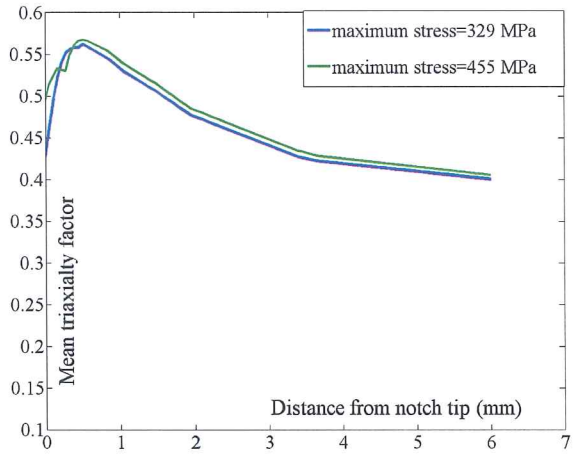

Figure 13. Evolution of mean triaxiality factor with distance from notch tip, for R=0.5, FE computation

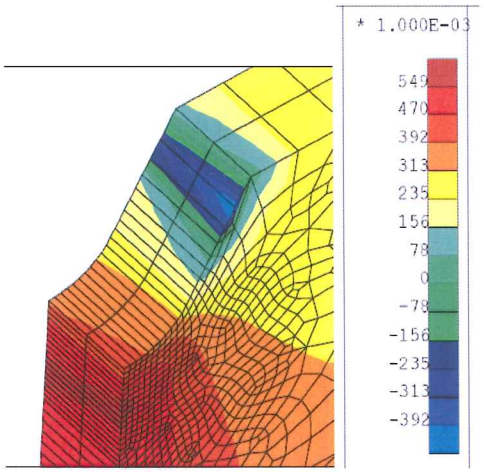

Figure 14. Distribution of the maximum triaxiality factor, for maximum stress=294 MPa, R=0.5, for V-notched sample

life (the fatigue behavior of Ti-6Al-4V contains important scatter in the experimental data).

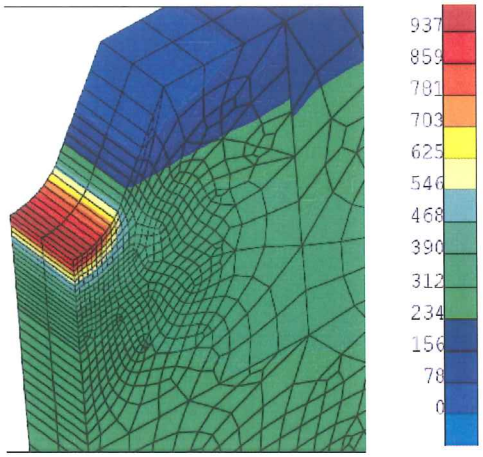

Figure 15. Distribution of the maximum Hill equivalent stress, for maximum stress=294 MPa, R=0.5, for V-notched sample

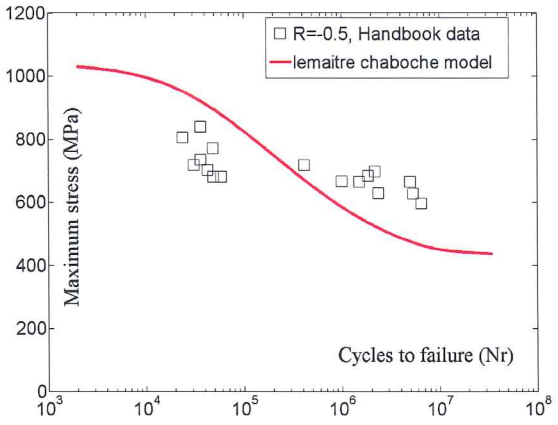

Figure 16. SN curve FE simulation, for R =-0.5, unnotched specimen, 1D loading

8.2. Results of multiaxial case

The simulated results by fatigue damage model of different stress ratio for V-notched samples were compared with experimental tests as shown

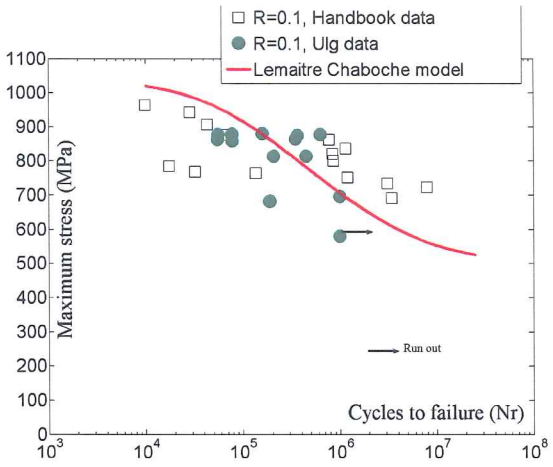

Figure 17. SN curve FE simulation, for R =0.1, unnotched specimen, 1D loading

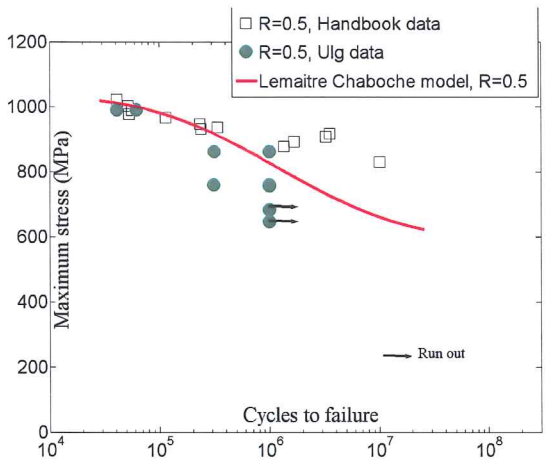

Figure 18. SN curve FE simulation, for R =0.5, unnotched specimen, 1D loading

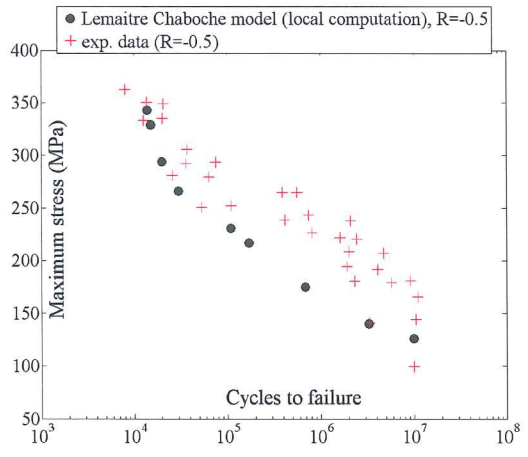

Figure 19. SN curve FE simulation, for R=-0.5,V-notched specimen

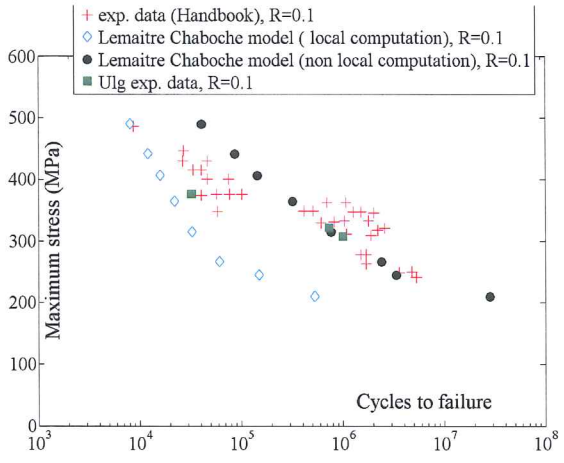

Figure 20. SN curve FE simulation, for R =0.1,V-notched specimen

in Figures (19), (20) and (21). It was observed that simulation of SN curves were in good agreement with experimental tests when the model is corrected by the stress gradient effect for the stress ratios R=0.1 and R=0.5 (tensile fatigue tests). The same remark is observed for the holed plate with R=0.54 (figure 23).

When the fatigue model is used locally (at the notch tip), the fatigue life predicted is lower than the fatigue life obtained by the fatigue test for the experiments with positive stress ratios ($R > 0$).

The model gives satisfactory results for the

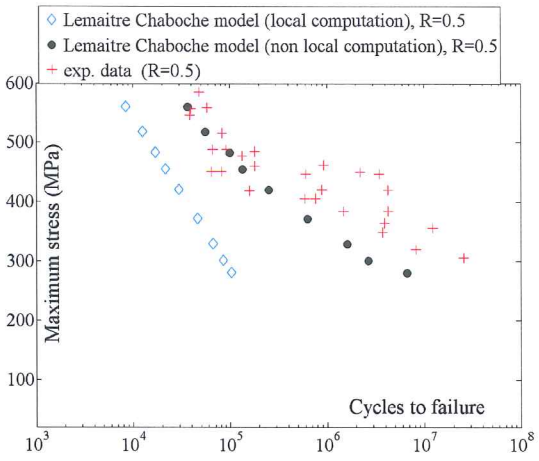

Figure 21. SN curve FE simulation, for R =0.5,V-notched specimen

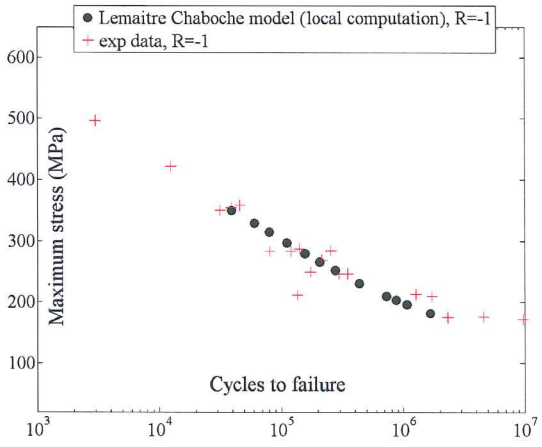

Figure 22. SN curve FE simulation without stress gradient computation R=-1, holed plate

negative stress ratios R=-0.5 (for V-notch,figure 19), R=-1 (for holed plate, figure 22), the mean triaxality factor is zero for negative stress ratios (no evolution of the damage under compressive part of the cycle load), the gradient computation for negative stress ratio is not necessary (in this case R=-1 and R=-0.5).

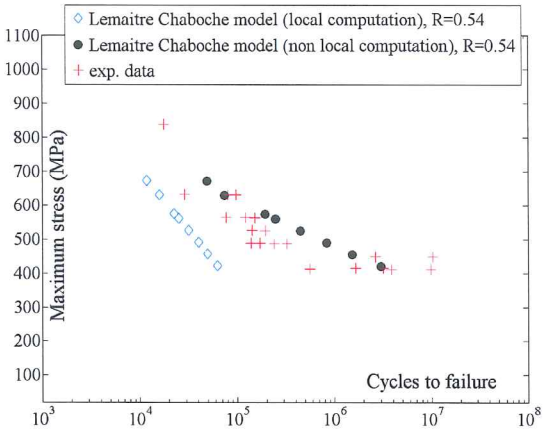

Figure 23. SN curve FE simulation without stress gradient computation R=0.54, holed plate

If the stress ratio increases, the difference between the experiments and simulation increases. In fact the local computation (at the notch tip) of the fatigue model gives a conservative results and the stress gradient in fatigue tensile case (R=0.1, R=0.5) is a key factor for the correct life prediction.

9. Conclusion

Fatigue model formulated using a continuum damage mechanics represent an important alternative to traditional approaches to fatigue, like Lemaitre Chaboche model. The results may be summarized in the following points :

- Teodosiu hardening law is a representative behavior law for Ti-6Al-4V. Note that for most simulated stress levels, there was an elastic stabilization after the first yielding (for tensile fatigue test, for fatigue life between 10^4 to 10^7).
- Lemaitre and Chaboche fatigue damage model gives a correct fatigue life prediction when the stress is homogenous in the sample ($K_t = 1$) or for no homogenous case, when the stress ratio is negative.
- Lemaitre and Chaboche fatigue damage mo-

del gives a conservative results in the case of notched specimens (for tensile fatigue tests with $R > 0$). The modified model was obtained by the introduction of the stress gradient in the fatigue life equation.

Acknowledgements

The authors acknowledge the Interuniversity Attraction Poles Programme- Belgian State- Belgian Scientific Policy(Contract P6/24). A.M.H and L.D. also acknowledge the Belgian Fund for Scientific Research FRS-FNRS for its support.

REFERENCES

[1] MIL-HDBK-5H : Metallic Materials and Elements for Aerospace Vehicle Structures. 1998

[2] Armstrong, P.J. and Frederick, C.O., "A Mathematical Representation of the Multiaxial Bauschinger Effect," Report RD/BfN 731, Central Electricity Generating Board. 1966.

[3] Flores, P., 2006, Development of experimental equipment and identification procedures for sheet metal constitutive laws. Ph.D. thesis, ULG, Liege.

[4] N.-A. Noda, M. Sera and Y. Takase. Stress concentration factors for round and flat test specimens with notches. Int. J.Fatigue Vol. 17, No. 3, pp. 163-178, 1995

[5] Jean Lemaitre, Jean-Louis Chaboche,Mechanics of Solid Materials. Cambridge University Press, New Ed, 25 August 1994.

[6] Chaudonneret. Simple efficient multixaxial fatigue damage model for engineering applications macro crack initiation. CNRS 1993.

[7] Sines, G., Behavior of metals under complex static and alternating stresses. Metal Fatigue, ed. G. Sines and J. L. Waisman. McGraw Hill, New York, 1959, pp. 145-169.

[8] L. Duchene, T. Lelotte, P. Flores, S. Bouvier. A.-M. Habraken. Rotation of axes for anisotropic metal in FEM simulations. International Journal of Plasticity 24 (2008)397427

[9] P. Jetteur, S. Cescotto.A Mixed Finite Element for the Analysis of Large Inelastic Strains.Int. Jl. Numerical Methods in Engineering, Vol. 31, 229-239, 1991.

[10] I. V. Papadopoulos. Invariant formulation of gradient dependent multiaxial high cycle fatigue criterion.Engineering Fracture Mechanics Vol. 55, No. 4, pp. 513-528, 1996.

[11] Y. Nadot, T. Billaudeau. Multiaxial fatigue limit criterion for defective materials. Engineering Fracture Mechanics 73 (2006) 112133

[12] Weixing Yao, Bin Ye, Lichun Zheng. A verification of the assumption of anti-fatigue design. International Journal of Fatigue 23 (2001) 271277.

[13] Qylafku G, Azari Z, Kadi N, Gjonaj M, Pluvinage G. Application of a new model proposal for fatigue life prediction on notches and key-seats. Int J Fatigue 1999;21 :75360.

[14] Bonora et al. Low cycle fatigue life estimation for ductile matals using a nonlinear continuum damage mechanics model. Int. Z Solids Structures Vol. 35, No. 16, pp. 1881-1894, 1998

[15] R. Desmorat a, S. Otin a,b. Cross-identification isotropic/anisotropic damage and application to anisothermal structural failure. Engineering Fracture Mechanics 75 (2008) 34463463.